

This is the peer reviewed version of the following article:

Crassiflorone derivatives that inhibit *Trypanosoma brucei* glyceraldehyde-3-phosphate dehydrogenase (TbGAPDH) and *Trypanosoma cruzi* trypanothione reductase (TcTR) and display trypanocidal activity / Uliassi, Elisa; Fiorani, Giulia; Krauth-Siegel, R. Luise; Bergamini, Christian; Fato, Romana; Bianchini, Giulia; Carlos Menéndez, J.; Molina, Maria Teresa; López-Montero, Eulogio; Falchi, Federico; Cavalli, Andrea; Gul, Sheraz; Kuzikov, Maria; Ellinger, Bernhard; Witt, Gesa; Moraes, Carolina B.; Freitas-Junior, Lucio H.; Borsari, Chiara; Costi, Maria Paola; Bolognesi, Maria Laura. - In: EUROPEAN JOURNAL OF MEDICINAL CHEMISTRY. - ISSN 0223-5234. - 141:(2017), pp. 138-148. [10.1016/j.ejmech.2017.10.005]

Terms of use:

The terms and conditions for the reuse of this version of the manuscript are specified in the publishing policy. For all terms of use and more information see the publisher's website.

18/12/2025 11:09

Accepted Manuscript

Crassiflorone derivatives that inhibit *Trypanosoma brucei* glyceraldehyde-3-phosphate dehydrogenase (TbGAPDH) and *Trypanosoma cruzi* trypanothione reductase (TcTR) and display trypanocidal activity

Elisa Uliassi, Giulia Fiorani, R. Luise Krauth-Siegel, Christian Bergamini, Romana Fato, Giulia Bianchini, J. Carlos Menéndez, Maria Teresa Molina, Eulogio López-Montero, Federico Falchi, Andrea Cavalli, Sheraz Gul, Maria Kuzikov, Bernhard Ellinger, Gesa Witt, Carolina B. Moraes, Lucio H. Freitas-Junior, Chiara Borsari, Maria Paola Costi, Maria Laura Bolognesi

PII: S0223-5234(17)30797-3

DOI: [10.1016/j.ejmech.2017.10.005](https://doi.org/10.1016/j.ejmech.2017.10.005)

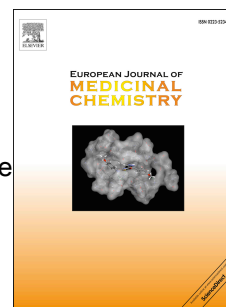
Reference: EJMECH 9797

To appear in: *European Journal of Medicinal Chemistry*

Received Date: 8 July 2017

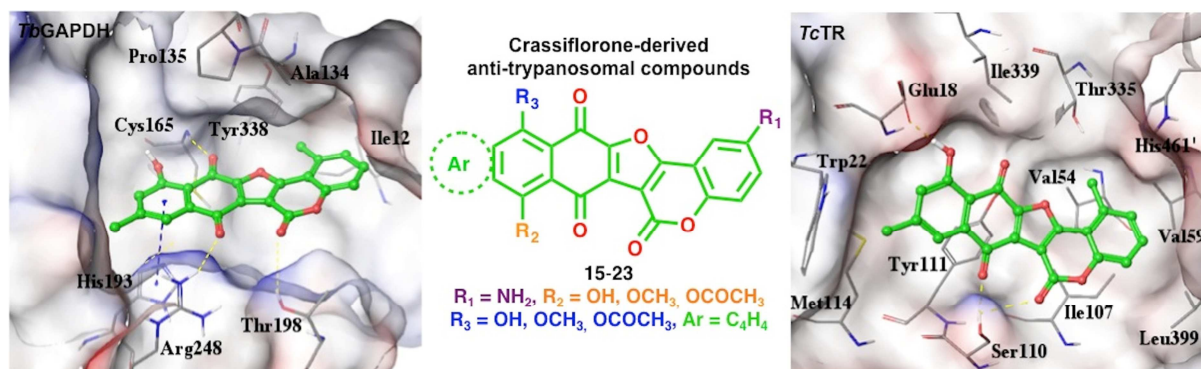
Revised Date: 18 September 2017

Accepted Date: 2 October 2017



Please cite this article as: E. Uliassi, G. Fiorani, R.L. Krauth-Siegel, C. Bergamini, R. Fato, G. Bianchini, J.C. Menéndez, M.T. Molina, E. López-Montero, F. Falchi, A. Cavalli, S. Gul, M. Kuzikov, B. Ellinger, G. Witt, C.B. Moraes, L.H. Freitas-Junior, C. Borsari, M.P. Costi, M.L. Bolognesi, Crassiflorone derivatives that inhibit *Trypanosoma brucei* glyceraldehyde-3-phosphate dehydrogenase (TbGAPDH) and *Trypanosoma cruzi* trypanothione reductase (TcTR) and display trypanocidal activity, *European Journal of Medicinal Chemistry* (2017), doi: 10.1016/j.ejmech.2017.10.005.

This is a PDF file of an unedited manuscript that has been accepted for publication. As a service to our customers we are providing this early version of the manuscript. The manuscript will undergo copyediting, typesetting, and review of the resulting proof before it is published in its final form. Please note that during the production process errors may be discovered which could affect the content, and all legal disclaimers that apply to the journal pertain.



Crassiflorone derivatives that inhibit *Trypanosoma brucei* glyceraldehyde-3-phosphate dehydrogenase (*Tb*GAPDH) and *Trypanosoma cruzi* trypanothione reductase (*Tc*TR) and display trypanocidal activity

Elisa Uliassi,^a Giulia Fiorani,^{a, b} R. Luise Krauth-Siegel,^b Christian Bergamini,^a Romana Fato,^a Giulia Bianchini,^c J. Carlos Menéndez,^c Maria Teresa Molina,^d Eulogio López-Montero,^d Federico Falchi,^{a, e} Andrea Cavalli,^{a, e} Sheraz Gul,^f Maria Kuzikov,^f Bernhard Ellinger,^f Gesa Witt,^f Carolina B. Moraes,^g Lucio H. Freitas-Junior,^g Chiara Borsari,ⁱ Maria Paola Costi,ⁱ and Maria Laura Bolognesi^{*a}

^a *Department of Pharmacy and Biotechnology, University of Bologna, Via Belmeloro 6 and Via Irnerio 48, 40126 Bologna, Italy*

^b *Biochemie-Zentrum der Universität Heidelberg, Im Neuenheimer Feld 328, 69120 Heidelberg, Germany*

^c *Departamento de Química Orgánica y Farmacéutica, Facultad de Farmacia, Universidad Complutense, Plaza de Ramón y Cajal, 28040 Madrid, Spain*

^d *Instituto de Química Médica (IQM-CSIC), c/Juan de la Cierva 3, 28006 Madrid, Spain*

^e *CompuNet, Istituto Italiano di Tecnologia, Via Morego 30, 16163 Genova, Italy*

^f *Fraunhofer Institute for Molecular Biology and Applied Ecology Screening Port, D-22525 Hamburg, Germany*

^g *Laboratório Nacional de Biociências (LNBio), Centro Nacional de Pesquisa em Energia e Materiais (CNPEM), SP13083-100 Campinas, Brazil*

ⁱ *Department of Life Sciences, University of Modena and Reggio Emilia, Via Campi 103, 41125 Modena, Italy*

^{*} Corresponding author: e-mail, marialaura.bolognesi@unibo.it

Abstract

Crassiflorone is a natural product with anti-mycobacterial and anti-gonorrhoeal properties, isolated from the stem bark of the African ebony tree *Diospyros crassiflora*. We noticed that its pentacyclic core possesses structural resemblance to the quinone-coumarin hybrid **3**, which we reported to exhibit a dual-targeted inhibitory profile towards *Trypanosoma brucei* glyceraldehyde-3-phosphate dehydrogenase (*Tb*GAPDH) and *Trypanosoma cruzi* trypanothione reductase (*Tc*TR). Following this basic idea, we synthesized a small library of crassiflorone derivatives **15-23** and investigated their potential as anti-trypanosomatid agents. **19** is the only compound of the series showing a balanced dual profile at 10 μ M (% inhibition_{*Tb*GAPDH} = 64% and % inhibition_{*Tc*TR} = 65%).

In phenotypic assay, the most active compounds were **18** and **21**, which at 5 μ M inhibited *Tb* bloodstream-form growth by 29% and 38%, respectively. Notably, all the newly synthesized compounds at 10 μ M did not affect viability and the status of mitochondria in human A549 and 786-O cell lines, respectively. However, further optimization that addresses metabolic liabilities including solubility, as well as cytochromes P450 (CYP1A2, CYP2C9, CYP2C19, and CYP2D6) inhibition, is required before this class of natural product-derived compounds can be further progressed.

Key words: coumarins, crassiflorone, glyceraldehyde-3-phosphate dehydrogenase, leishmaniasis, natural products, quinones, trypanocidal activity, trypanosomiasis, trypanothione reductase.

Introduction

Trypanosomatid parasites cause a number of highly debilitating and potentially fatal neglected tropical diseases that significantly impact human health [1-3]. They include human African trypanosomiasis (HAT), commonly called sleeping sickness, caused by two parasites of the genus *Trypanosoma*, i.e. *T. brucei gambiense* and *T. brucei rhodesiense*. The former is responsible for a chronic form of HAT in Central and Western Africa, while the latter causes an acute disease in Southern and Eastern Africa. *Trypanosoma cruzi* is another trypanosomatid parasite that is responsible for Chagas disease, an infection that affects about 200,000 people per year in South America. Furthermore, leishmaniasis is a widespread trypanosomatid disease caused by over 20 species of the genus *Leishmania* [1]. Most of the cases occur in the Indian subcontinent, East Africa and Brazil, but elevated incidences are reported from several other countries of South America, Southern Mediterranean, Middle East and Central Asia [4]. Importantly, co-infection with *Leishmania* spp. and HIV is expected to increase disease burden and severity, and recent refugee movements from the Middle East into Europe are likely to spread leishmaniasis in Europe [1].

The currently available drugs by no means reflect the clinical need, as they are often plagued by toxic side effects, lack of efficacy, development of resistance, prolonged treatment duration and complex drug administration procedures [2]. Thus, new drugs are required, especially those that are appropriate for rural health systems, in resource-poor settings [1].

In this context, natural products (NPs) represent an untapped resource for novel, diverse, safe, and affordable anti-trypanosomatid lead compounds [5]. Indeed, NPs serve as a valuable source for novel molecular scaffolds in drug development. Around 65% of all approved drugs are classified as NPs or are inspired by an NP core [6]. Therefore, NPs have the advantage of offering novel structural classes of drugs because of their well-documented, expanded coverage of chemical space relative to synthetic compounds [7, 8]. It is worth noting that amphotericin B and paromomycin are prominent examples of NPs used against leishmaniasis [3].

In addition, NPs often act as plant and animal defense chemicals with an intrinsic multitarget mechanism of action [9, 10]. Due to the processes that nature uses for their generation, NPs usually possess a complex structure with an array of functional groups. Thus, their biosynthetic pathways involve a range of enzymes, each with distinct topology and binding sites, to which the NP under construction needs to bind. As a result of this mode of generation, NPs have an inherited propensity to recognize multiple target proteins [10, 11].

Based on the above considerations, as well as on our continuous interest in multitarget compounds directed against two anti-trypanosomatid drug targets [12], namely *Trypanosoma brucei* glyceraldehyde-3-phosphate dehydrogenase (*Tb*GAPDH) [13] and *Trypanosoma cruzi* trypanothione reductase (*Tc*TR) [14], we turned our attention to NP crassiflorone (**1**) (see Fig. 1). **1** is a pentacyclic furocoumarin naphthoquinone isolated from the African ebony *Diospyros crassiflora* [15], with reported anti-mycobacterial and anti-gonorrhoeal activities [16]. To note, following the total synthesis of **1**, some doubt has been cast on the structure of crassiflorone, which might be a regioisomer of **1**, although a direct comparison with the natural material was not possible [24].

We envisaged that **1** could act as a potential dual GAPDH/TR inhibitor. This proposal was based on the fact that its scaffold shares the same structural features of dual-targeted inhibitors previously identified by us [12]. In particular, starting from the dual-targeted 2-phenoxy-naphthoquinone fragment **2** (*Tb*GAPDH IC_{50} = 7.2 μ M and *Tc*TR IC_{50} = 9.0 μ M) [17, 18], we had developed dual inhibitors exemplified by the quinone-coumarin hybrid **3** (*Tb*GAPDH IC_{50} = 5.4 μ M and *Tc*TR K_i = 2.3 μ M) [12]. Hence, we reasoned that **1**, similarly featuring both the quinone and coumarin frameworks, could be a good starting point for the development of novel NP-inspired GAPDH/TR inhibitors (Fig. 1).

2. Design rationale

Building on this rationale, we aimed to verify whether **1** could bind at both enzyme active sites. According to the significant similarity within the Trypanosomatid family of the two selected proteins and their accessibility [19, 20], we performed docking analysis on *Tb*GAPDH (PDB 2X0N) [21] and *Tc*TR (PDB 1BZL) [22]. The docking results showed that **1** recognizes *Tb*GAPDH by establishing favorable interactions (Fig. 1). In particular, both the coumarin and naphthoquinone frameworks of **1** are involved in the formation of a network of H-bonds, between the carbonyl of lactone ring with the side chain of Thr198 (4.0 Å), and both the carbonyl groups of quinone with the backbone of Cys165 (2.0 Å) and the side chain of Arg248 (2.1 Å). In addition, the pentacyclic aromatic scaffold establishes π - π interaction with His193 (4.2 Å) and favorable hydrophobic interactions with Tyr338. On the other hand, the wide and hydrophobic cavity of TR nicely accommodates **1**, primarily anchored by π - π interactions with Tyr111 (2.9 Å). Hydrogen bonds could be identified between both the carbonyl groups of the coumarin and quinone frameworks of **1** and Ser110 (1.8 Å and 2.2 Å, respectively), and between the hydroxyl substituent of **1** and Glu19 (1.6 Å) (Fig. 1). Moreover, the hydrophobic interactions with Trp22, Val54, Val59, Ile107, Met114, Ile339, and Leu399' further contribute to stabilize the binding of **1**. Thus, docking studies predicted that such a bulky and rigid scaffold interacts with both targets of interest, confirming the design rationale.

On this basis, we designed a small series of **1**-derived compounds, which, for reasons of synthetic accessibility, do not carry the methyl substituents on the pentacyclic core. Our goal was to identify the substitution pattern of **15** (see Scheme 2) that would preserve target recognition, while simultaneously modulating lipophilicity and solubility. Thus, we introduced hydroxyl (as in **1**), methoxy and acetoxy substituents at positions 8 and 11 (**17-22**) to increase polarity and to disrupt the molecular planarity of **15**. Additionally, the anthraquinone derivative **16**, as an extension of the naphthoquinone skeleton at positions 9 and 10, has been included in the series. Along the same lines, we envisaged the introduction in position 2 of an amino group (**23**).

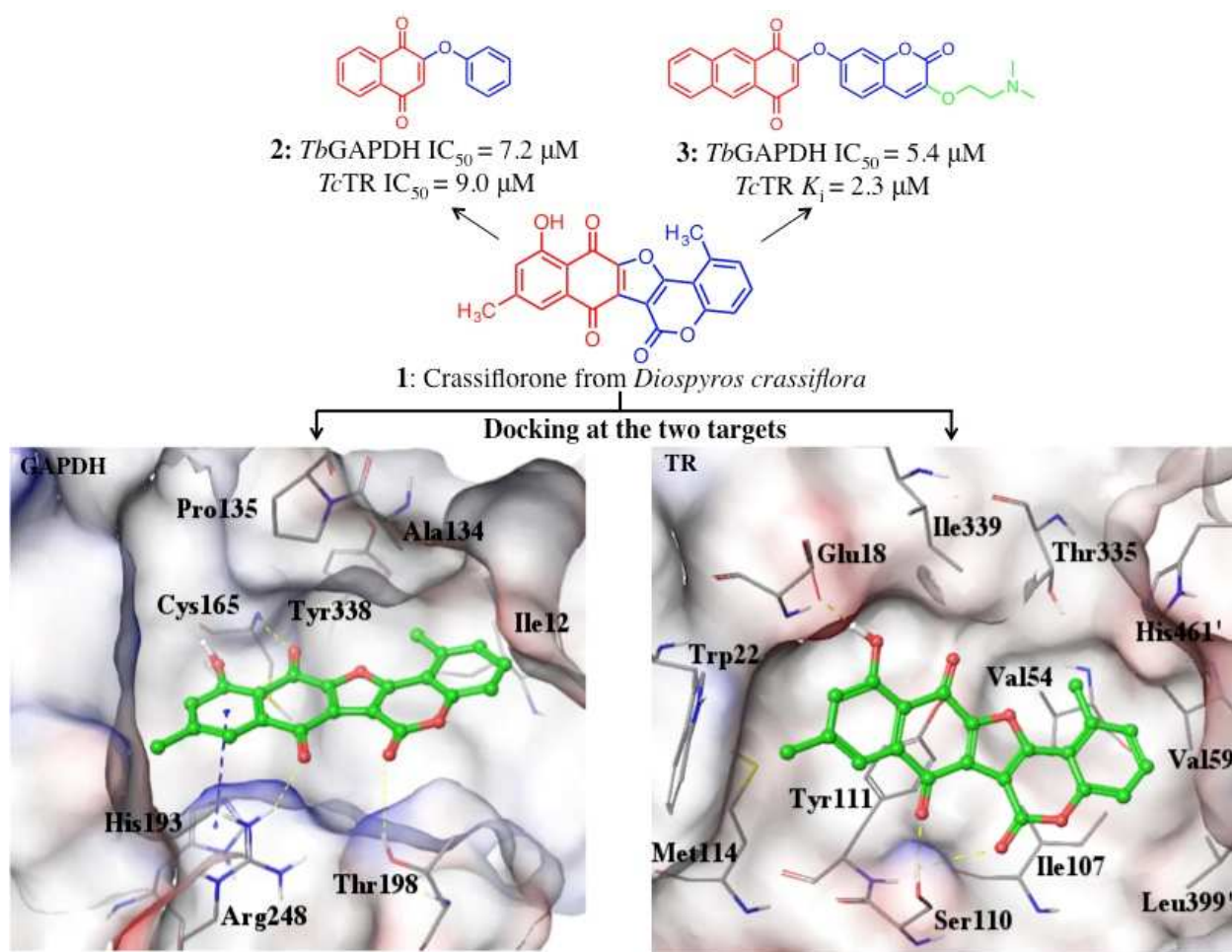
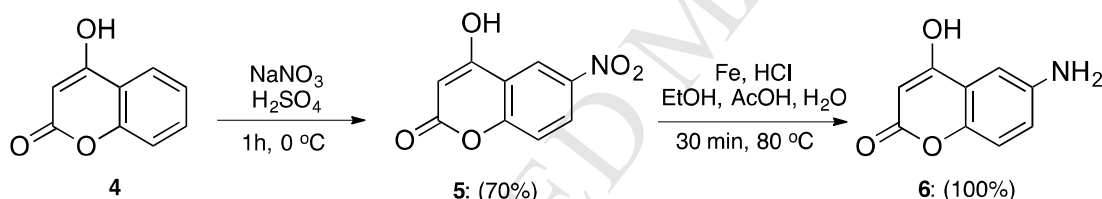


Fig. 1. Design strategy to crassiflorone-derivatives **15-23** and putative binding modes of **1** at the *Tb*GAPDH (left panel, PDB 2X0N) and *Tc*TR (right panel, PDB 1BZL) active sites. Primed residues belong to the second subunit of the homodimeric TR. The yellow dotted lines represent hydrogen bonds, and blue dotted lines show π - π interactions.

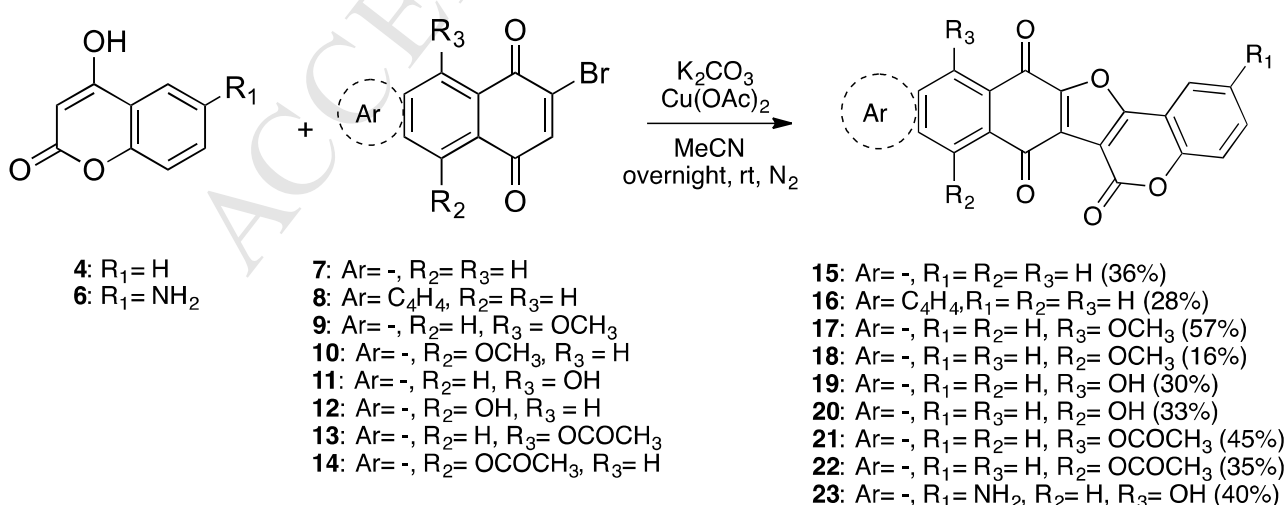
3. Chemistry

For the synthesis of **15-23**, the same retrosynthetic approach reported for **1**, starting from 4-hydroxycoumarin and 2-bromonaphthoquinone derivatives as precursor structures, was exploited [23, 24]. Accordingly, the preparation of intermediate coumarin **6** and quinones **7-14** was required. As shown in Scheme 1, the nitration of the commercially available **4** with potassium nitrate and concentrated sulfuric acid at 0 °C gave compound **5** [25], which was reduced by using iron powder in a mixture of ethanol/acetic acid/hydrochloric acid/water, furnishing **6** in a quantitative yield. 2-

Bromonaphthoquinones **7-14** were synthesized as previously described [26, 27]. With both intermediates **4**, **6**, **7-14** in hand, we followed the reported coupling reaction in the presence of potassium carbonate and copper(II) acetate to easily afford **15-23** in moderate to good yields (16-57%, Scheme 2) [23, 24]. This one-pot procedure allowed the efficient coupling between the two precursor structures under mild reaction conditions (i.e. weak base and room temperature). The nucleophilic attack of enolate anions formed through the base-mediated deprotonation of the hydroxyl groups of **4** and **6** onto the more electrophilic carbon atom of **7-14** is followed by the copper(II) mediated-oxidative cyclization of the resulting intermediate adducts, which represents the thermodynamic driving force for the ring closure and subsequent aromatization to directly provide the pentacyclic scaffold. Compounds **15-23** thus obtained were characterized by $^1\text{H-NMR}$ and high-resolution mass spectra (see the Experimental Section).



Scheme 1. Synthesis of coumarin intermediate **6**.



Scheme 2. Synthesis of crassiflorone derivatives **15-23**.

4. Results and discussion

To investigate the anti-trypanosomal profile, crassiflorone derivatives **15-23** were characterized for their enzymatic (*Tb*GAPDH and *Tc*TR) and whole-cell parasite (*L. infantum*, *T. brucei* and *T. cruzi*) activities. In addition, assessment of their *in-vitro* early-toxicity profile was carried out.

4.1 *Tb*GAPDH inhibition studies

We tested the inhibitory activity of **15-23** against *Tb*GAPDH at a concentration of 10 μ M, following a previously reported protocol [28]. The collected percentages of enzymatic inhibition are graphically reported in Fig. 2A, in comparison with **2**. Notably, among the synthesized compounds, **18**, **19** and **23** showed inhibition percentages higher than 50% and higher to that observed for **2**. Particularly, the most active compounds were the 8-OMe-substituted derivative (88%) (**18**) and the amino-coumarin derivative **23** (75%). In spite of the promising results, the poor solubility of **18** prevented further measuring its inhibitory activity at different (higher) concentrations, due to compound precipitation in the assay. The same applied to **19**. For the more soluble **23**, the dose-response curve was determined and the IC₅₀ value was found to be 2.1 μ M (Fig. 2B). Importantly, **23** turned out to be more active than the corresponding “open analogue” **3** (IC₅₀ *Tb*GAPDH = 5.4 μ M) [16], demonstrating that the molecular rigidification strategy applied resulted in a better *Tb*GAPDH recognition. Moreover, these values place **23** as the most active *Tb*GAPDH inhibitor reported so far, being more active than other identified natural and unnatural compounds [29-31]. Notably, docking studies suggest that **23** interacts at the *Tb*GAPDH active site through additional H-bonds between the -OH group and the backbone of Asn334 (1.9 Å) and between the -NH₂ and the side chain of Thr166 (1.7 Å), which are not present in **1**/*Tb*GAPDH complex (Fig. 2C left panel). Furthermore, **23** is stabilized by favorable π - π and π -cation interactions. Conversely, the lack of inhibitory activity of anthraquinone **16**, and acetoxo derivatives **21** and **22** may be ascribed to their higher steric hindrance. In fact, they showed no inhibitory effect on *Tb*GAPDH up to 10 μ M

(data not shown). Collectively, the introduction of small substituents on both quinone and coumarin scaffolds seems to positively modulate the anti-*Tb*GAPDH profile of this small set of crassiflorone derivatives.

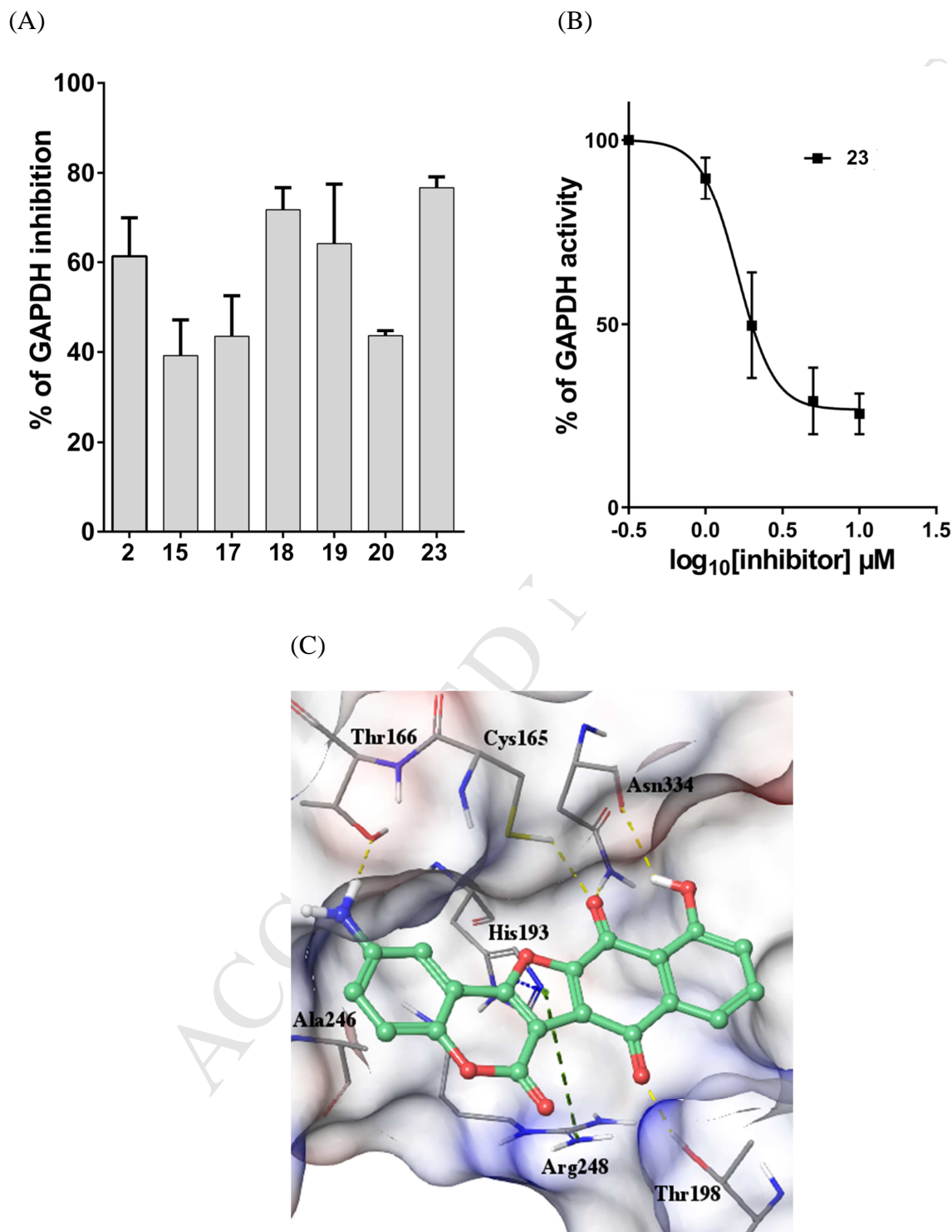


Fig. 2. (A) Percentages of *Tb*GAPDH inhibition by compounds **15**, **17-20**, **23**, and **2**. The activities were measured spectrophotometrically by following NAD reduction, and data are the means \pm SEM

of three determinations. (B) *Tb*GAPDH inhibition curve by compound **23** ($IC_{50} = 2.1 \mu M$). (C) Putative binding mode of **23** at the active site of *Tb*GAPDH (PDB 2X0N). The yellow dotted lines represent hydrogen bonds, green dotted lines are used for π -cation interactions and blue dotted lines show π - π interactions.

4.2 *Tc*TR inhibition studies

In parallel, we determined the *Tc*TR inhibition profile of **15-23** at the highest concentrations soluble in the assay buffer, as previously described [32]. At a concentration of 100 μM or 40 μM of trypanothione disulfide (TS_2), which correspond to a substrate concentration of $6 \times K_m$ and $2.4 \times K_m$, respectively [33], 10 μM of anthraquinone **16** and -OMe derivative **18** showed negligible inhibitory activity ($< 20\%$), whereas **23** turned out to be totally inactive, even at a concentration of 100 μM (Table 1). Unfortunately, the unsubstituted compound **15** could be tested only at 5 μM concentration, yielding a *Tc*TR inhibition percentage of about 20% at both TS_2 concentrations. In contrast with what was observed for *Tb*GAPDH, **21** and **22**, carrying the acetoxy substituent in positions 8 or 11, moderately inhibited *Tc*TR ($\approx 40\%$ of *Tc*TR inhibition at both substrate concentrations). In this respect, the extended dimension and permissiveness of the *Tc*TR active site compared to that of *Tb*GAPDH likely allow the proper fitting of **21** and **22**. Furthermore, docking studies suggest a potential role of the electron-donor acetoxy group of **22** in the formation of a H-bond with Tyr111 (1.8 Å) and several π - π interactions made by the coumarin framework and Trp22 and Tyr111 (Fig. 4). Notably, compounds **17** and **19** displayed percentage of *Tc*TR inhibition (at 40 μM of substrate) ranging from 42.6% to 65% when tested at 20 μM and 10 μM , respectively. The degree of *Tc*TR inhibition shown by compounds **17**, **21** and **22** at two different concentration of TS_2 was essentially identical (Table 1). This was a first indication that the compounds did not act as purely competitive inhibitor of the enzyme.

Table 1. Inhibition of *TcTR* by compounds **15-23**. The activities were measured spectrophotometrically following the decrease in absorbance over time at 340 nm due to NADPH consumption and the percentage of inhibition was calculated. The data are the average of two independent determinations that differed by $\leq 5\%$.

| Compound | [Inhibitor] (μM) | % Inhibition of <i>TcTR</i> at | |
|----------------------|-------------------------------|-----------------------------------|----------------------------------|
| | | TS ₂ 100 μM | TS ₂ 40 μM |
| 15 | 5 | 18 | 19.1 |
| 16 | 10 | 7.9 | 2.1 |
| 17 | 20 | 41.1 | 42.6 |
| 18 | 10 | 8.1 | 20.6 |
| 19 | 10 | 37.8 | 65 |
| 20 | 2.5 | 11.6 | 42.9 |
| 21 | 5 | 35.2 | 41 |
| 22 | 10 | 37 | 37.2 |
| 23 | 100 | - | - |
| 2^a | 10 | 29 | 23 |

^a Data taken from ref [12].

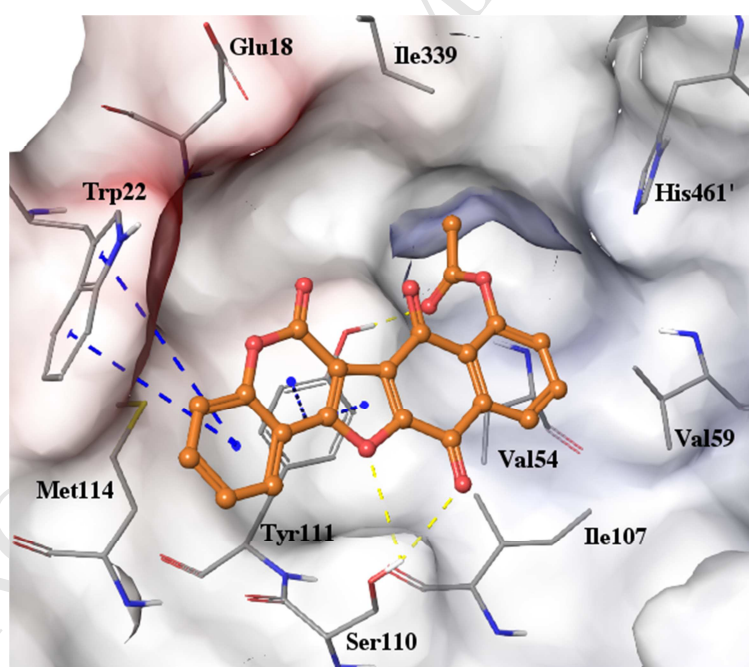


Fig. 4. Putative binding mode of **22** at the active site of *TcTR* (PDB 1BZL). The yellow dotted lines represent hydrogen bonds, and blue dotted lines show π - π interactions.

To further investigate the inhibitory mechanism, two of the most potent inhibitors **17** and **19** were subjected to a detailed kinetic analysis. The double-reciprocal plots (Fig. 5) revealed that **17** inhibits *Tc*TR non-competitively with a K_i value of $22.4 \pm 1.9 \mu\text{M}$, whereas compound **19** showed a mixed type inhibition with K_i values of 5.6 ± 1.9 . Gratifyingly, in the case of **19**, the K_i value is in the range of many well-known TR inhibitors, such as clomipramine [34] and 5-{5-[1-(pyrrolidin-1-yl)cyclohexyl]-thien-2-yl}-1*H*-indole [35] (K_i values of $6.5 \pm 0.6 \mu\text{M}$ and $4 \pm 1 \mu\text{M}$, respectively, under the same experimental conditions). In addition, **19** is the only compound of the series showing a balanced dual profile at $10 \mu\text{M}$ (% inhibition_{*Tb*GAPDH} = 64% and % inhibition_{*Tc*TR} = 65%).

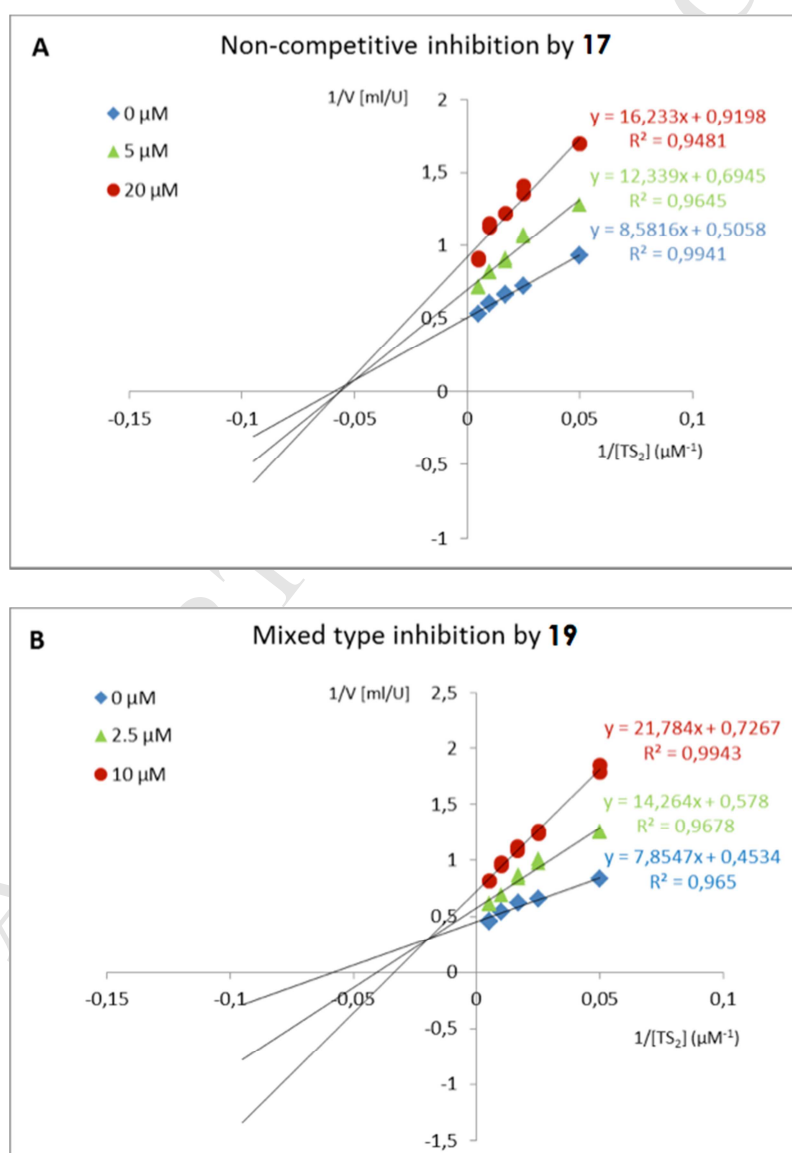


Fig. 5. Lineweaver–Burk plots for the inhibition of *Tc*TR by **17** (A) and **19** (B). The assays were performed at two fixed concentrations of inhibitor as indicated in the graph, and the TS_2

concentration was varied. All assays in the presence of inhibitor were conducted at least in duplicate. The inhibitor constants were derived from a direct plot (for details see the Experimental section). The K_i -values for **17** and **19** were $22.4 \pm 1.9 \mu\text{M}$ and $5.6 \pm 1.9 \mu\text{M}$, respectively. The α -values for compound **19** was 2.7 ± 1.4 .

4.2 Whole-cell parasite assays

Compounds **15-23** were tested against *T. brucei* bloodstream, *T. cruzi* intracellular trypomastigote, and *L. infantum* intracellular amastigote forms (Fig. 6). The compounds were tested at the highest concentrations soluble in the assay buffer. An analysis of the collected data highlights no or negligible activity against *T. cruzi* trypomastigote and *L. infantum* amastigote forms, whereas *T. brucei* bloodstream parasite was more susceptible to the compounds. In fact, **18** and **21** showed good 29% and 38% of *Tb* growth inhibition at $5 \mu\text{M}$. However, determination of their activity at higher concentrations was not possible due to solubility problems. Notably, in the case of more soluble (under the experiment conditions) NH_2 -substituted **23** that could be successfully tested at $50 \mu\text{M}$, a significant inhibition of 77% of *Tb* growth can be appreciated. Unexpectedly, dual-targeted **19** showed negligible inhibition ($< 20\%$ at $10 \mu\text{M}$) of the three parasites growth, which makes it less active than single-targeted *Tb*GAPDH **18** and *Tc*TR **21** inhibitors.

Clearly, for the current series of crassiflorone analogues, the anti-trypanosomatid profile is the result of both pharmacokinetic and pharmacodynamic features. In fact, the lack of correlations between enzymatic and cellular activities within the series may be (at least partially) ascribed to the fact that their activity is a result of diffusion across the plasma membrane (highly dependent on solubility and parasite under study), intracellular targeting into different cellular organelles (i.e. glycosome), and finally interaction with the selected molecular targets.

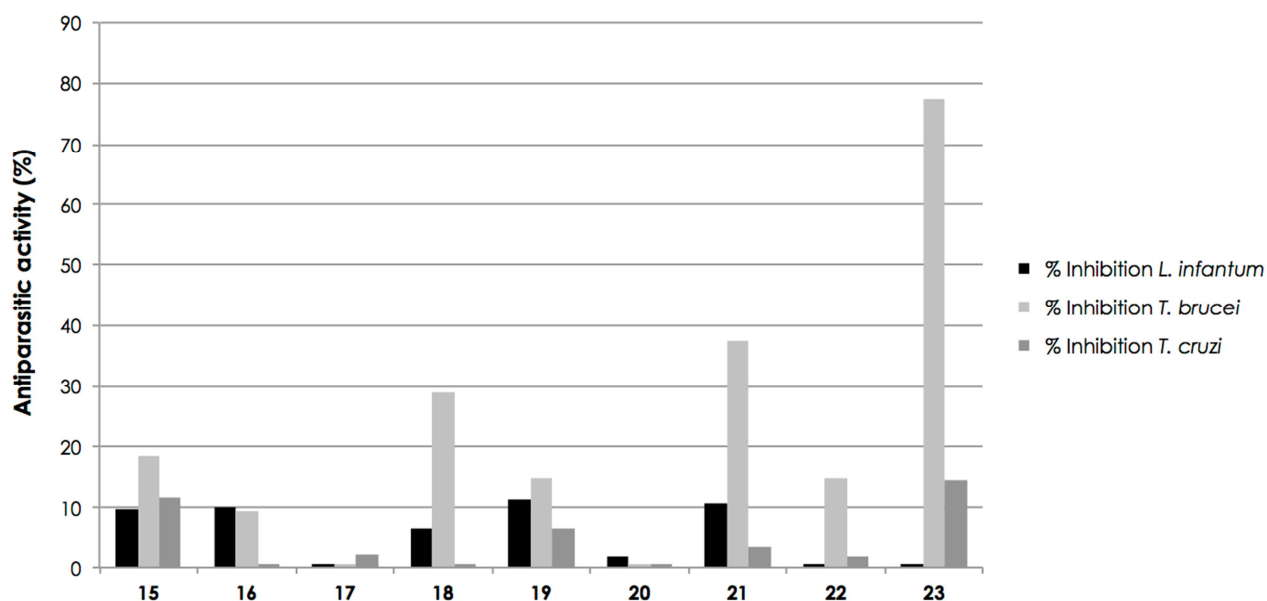


Fig. 6. Anti-parasitic activities of **15-23** against *L. infantum* (in black), *T. brucei* (in light gray) and *T. cruzi* (in dark gray). **16-18** and **20-22** were tested at 5 μ M, **15** at 12.5 μ M, **19** at 10 μ M and **23** at 50 μ M. The SD values agreed to $\pm 10\%$. The reference compounds were pentamidine ($EC_{50} = 5.3$ μ M) for *T. brucei*, amphotericin B for *L. infantum* ($EC_{50} = 1.5$ μ M), and benznidazole for *T. cruzi* ($EC_{50} = 43.7$ μ M).

4.5 In-vitro compound mediated early-toxicity assessment

In light of the poor drug-like properties and the scarce safety profile of the currently available anti-trypanosomatid drugs [1] as well as the liabilities of quinones [36], the *in-vitro* early-toxicity profiles [37] of **15-23** were determined for cytotoxicity (A549, human lung adenocarcinoma epithelial cell line), cytochrome P450 inhibition (CYP1A2, CYP2C9, CYP2C19, CYP2D6 and CYP3A4), mitochondrial toxicity (786-O, human renal carcinoma cell line) and hERG inhibition [38]. The output of these studies together with the phenotypic ones, are useful to make an informed decision as to which compounds should be progressed in further studies. The compounds were screened in each of the *in-vitro* early-toxicity assays at 10 μ M and a traffic light system was employed to rank the compounds such that green = no liability, yellow = medium liability and red = significant liability (Table 2).

The rationale for implementing the cytotoxicity assay was to establish whether the observed phenotypic effects were related to specific anti-parasitic activity and not merely due to toxicity to the host cell on which the parasites depend. Remarkably, none of the tested compounds inhibited the growth of the human A549 cell line at 10 μ M. This information added confidence that for the best-performing compounds, namely **18** and **21**, a certain degree of host/parasite selectivity could be reached.

The inhibition of the cytochrome P450 (CYP) enzymes is a major cause of drug-drug interactions [39] and in the case of anti-trypanosomatid compounds this is an issue, with co-morbidity (e.g. HIV infection) as a major problem for many diseased patients [40]. In this respect, we determined the inhibitory profiles of **15-23** at 10 μ M on five isoforms of CYP enzymes (CYP1A2, CYP2C9, CYP2C19, CYP2D6, and CYP3A4) [41]. Although **15-20** and **23** had no or medium liability against CYP3A4, the other compounds were associated with significant cytochrome P450 liabilities and this needs to be addressed in any further compounds of this class that are designed and synthesized.

Blockade of hERG K⁺ channel is important as can lead to cardiotoxicity, especially in the case of cardiomyopathy caused by Chagas disease [38], therefore it is important for any drug not be associated with this effect [42]. Notably, among the tested compounds at 10 μ M, only **19** and **21** were associated with significant hERG liability.







As mitochondrial toxicity by way of swelling and membrane potential collapse have been reported as a possible mode of trypanocidal action of naphthoquinone analogues [28, 43], and nonselective off-target mitochondrial toxicity [44] is a major contributor to the failure of quinone drugs, we tested whether **15-23** at 10 μ M could induce mitochondrial toxicity. Remarkably, all the synthesized compounds display no sign of mitochondrial toxicity at the tested concentration.

The above *in-vitro* early-toxicity assessment has demonstrated some liabilities of the crassiflorone scaffold and has led to the identification of those that need to be addressed when designing the next generation of derivatives.

Table 2. *In-vitro* compound mediated early-toxicity for **15-23**. The liabilities are ranked using a traffic light system such that green = no liability, yellow = medium liability and red = significant liability.^a

| Cmpds | % Inhibition hERG at 10 μ M \pm STD % | | % Inhibition CYP1A2 at 10 μ M \pm STD % | | % Inhibition, CYP2C9 at 10 μ M \pm STD % | | % Inhibition CYP2C19 at 10 μ M \pm STD % | | % Inhibition CYP2D6 at 10 μ M \pm STD % | | % Inhibition CYP3A4 at 10 μ M \pm STD % | | % Cell growth A549 at 10 μ M \pm STD % | | % Mitochondrial viability at 10 μ M \pm STD % | |
|-------|---|-------|---|------|--|------|--|------|---|------|---|-------|--|-------|---|-------|
| 15 | 20,33 | 6,22 | 48,19 | 1,94 | 32,35 | 6,79 | 46,09 | 5,16 | 70,99 | 0,75 | 14,80 | 2,81 | 145,63 | 50,81 | 89,15 | 29,02 |
| 16 | 9,77 | 9,62 | 38,54 | 3,02 | 42,43 | 4,21 | 35,71 | 8,59 | 54,95 | 6,78 | 7,93 | 2,16 | 139,80 | 38,06 | 89,59 | 19,02 |
| 17 | 42,72 | 29,55 | 99,15 | 0,17 | 89,34 | 2,66 | 55,45 | 4,70 | 108,20 | 0,51 | 38,48 | 1,73 | 165,75 | 64,67 | 89,95 | 28,07 |
| 18 | 57,98 | 15,03 | 87,21 | 0,64 | 61,60 | 2,42 | 71,05 | 1,72 | 100,56 | 5,20 | 22,11 | 10,01 | 130,42 | 22,26 | 96,22 | 13,16 |
| 19 | 67,12 | 28,69 | 57,27 | 1,75 | 61,55 | 1,12 | 106,64 | 0,44 | 101,91 | 0,72 | 40,81 | 8,31 | 138,23 | 37,66 | 82,16 | 9,92 |
| 20 | 19,48 | 3,14 | 40,77 | 1,94 | 44,60 | 1,74 | 83,78 | 3,48 | 95,19 | 0,33 | 9,44 | 8,27 | 166,70 | 46,39 | 85,82 | 16,20 |
| 21 | 86,84 | 21,40 | 93,48 | 1,47 | 99,25 | 0,61 | 109,41 | 0,32 | 107,52 | 0,42 | 88,65 | 2,92 | 182,96 | 46,16 | 90,52 | 14,03 |
| 22 | 4,02 | 2,21 | 94,59 | 0,92 | 92,52 | 2,11 | 102,90 | 1,63 | 105,99 | 0,36 | 88,18 | 3,13 | 156,60 | 17,48 | 98,86 | 1,76 |
| 23 | 7,99 | 20,77 | 37,77 | 2,01 | 85,92 | 0,86 | 63,64 | 1,17 | 71,50 | 4,51 | 46,77 | 6,35 | 156,91 | 41,47 | 97,94 | 16,34 |

^a Traffic light legend:

| | | | | | |
|------------------------------------|---|-------|--|---|-------|
| % inhibition of hERG, CYP isoforms |  | > 60% | % cell growth A549 and mitochondrial viability |  | < 0% |
| |  | < 60% | |  | < 60% |
| |  | < 30% | |  | > 60% |

4.6 Pan Assay Interference Compounds (PAINS) and solubility analyses

Due to the presence in **15-23** of chemical substructures that belong to the PAINS category [45], we have assessed their potential PAINS behavior using the FAF-Drugs4 filter (available on <http://fafdrugs3.mti.univ-paris-diderot.fr>) [46]. Not unexpectedly, our compounds were assessed to include high-risk (quinone) and low-risk (coumarin) structural alerts (data not shown). However, we are quite confident that **15-23** should not act as PAINS and their activity is not an artifact, because they showed no activity when tested in two parallel HTS assays against *Leishmania* and *Trypanosoma* pteridine reductase-1 (PTR-1) enzymes (see Supplementary Information, Table S1). In addition, to rule out that solubility issues might have affected the accuracy of the performed assays, target compounds **15-23** were evaluated for their aqueous solubility (Table S2). Solubility data included in silico calculations of LogS, performed by means of two different programs (i.e., MarvinSketch 17.13 and FAF-Drugs4), and experimental aqueous solubility determined by nephelometry. Encouragingly, all the compounds were tested at concentrations below the solubility limit.

5. Conclusions

Herein, for the first time the natural compound crassiflorone (**1**) has been proposed as a potential dual *Tb*GAPDH/*Tc*TR inhibitor and novel synthetic crassiflorone derivatives (**15-23**) have been designed and synthesized. In this respect, **15-23** were envisaged as rigid analogues of previously reported coumarin-quinone hybrids exemplified by **3** [12]. Among the tested compounds, only **19** displayed a balanced dual profile against the selected targets (% inhibition at 10 μ M *Tb*GAPDH = 64% and *Tc*TR = 65%). Unfortunately, this profile did not give rise to the expected superior anti-trypanosomal cellular activity. In fact, in the phenotypic assay, the best performing compounds of the series were single-targeted inhibitors **18** and **21**, which were more active than **19**. However, solubility concerns clearly affected the anti-trypanosomatid profile of these compounds.

Although we have identified liabilities of the crassiflorone scaffold in terms of solubility and CYP1A2, CYP2C9, CYP2C19, and CYP2D6 inhibition, the lack of cytotoxicity against human cells as well as mitochondria, points towards a possible developability of this class. In fact, we anticipate that it will be possible to overcome the current drawback in the next generation of compounds, as these problems are not likely to be insurmountable. For instance, with regards to the low solubility of the compounds, formulation technology (i.e. particle size reduction, spray drying and hot melt extrusion) can be investigated as this has been successfully implemented for class IV (low permeability, low solubility) compounds based upon the Biopharmaceutics Classification System [47].

6. Experimental section

6.1 Chemistry

6.1.1. General chemical methods

All reagents were obtained from commercial sources and used without further purification. Reactions were followed by analytical thin layer chromatography (TLC), performed on pre-coated TLC plates (layer 0.20 mm silica gel 60 with a fluorescent indicator UV254, Merck). Developed

plates were air-dried and analyzed under a UV lamp at 254/365 nm. Flash column chromatography was performed on silica gel (Kieselgel 40, particle size 0.040-0.063 mm, Merck). Compounds were named using ChemDraw Professional 15.0. The identity and purity of final compounds was assessed by ^1H -NMR and QTOF LC/MS system (Ascentis C18 column 250 mm \times 4.6 mm, 5 μm , Supelco, Bellefonte, PA, USA; gradient elution of (A) H_2O and (B) acetonitrile (from 25% B to 40% B); flow rate of 1.0 mL/min; sample injection volume was 5 μL). ^1H -NMR and ^{13}C -NMR spectra were recorded on Varian Gemini 400 or on Bruker Avance 250 spectrometers operating at 400/250 and 100/62.9 MHz for ^1H and ^{13}C -NMR spectra, respectively. Chemical shift (δ) values are given in ppm and are recorded using the residual non-deuterated solvent as an internal standard. The multiplicities are reported as: s (singlet), d (doublet), t (triplet), q (quartet), m (multiplet), br s (broad singlet), exch (exchangeable with D_2O) and doublet of doublet (dd). Coupling constants (J) are given in Hertz (Hz). As already reported for **1** and derivatives [23, 24], ^{13}C -NMR spectroscopic data for **15-23** are not available, due to their insufficient solubility in d_6 -DMSO. High-resolution mass spectra were obtained by using a Bruker FTMS APEX QIV mass spectrometer or 6520 Accurate-Mass QTOF LC/MS. Low-resolution mass spectra ESI-MS were recorded on a Waters ZQ 4000 apparatus. Melting points (m.p.) were measured on a Reichert 723 hot stage microscope or in glass capillary tubes on Buchi SMP-20 apparatus and are uncorrected.

Compounds **7-14** have been synthesized as previously reported and the spectroscopic data are in agreement with those reported in the literature [26, 27].

6.1.2. Synthesis of coumarin derivative **6**

6.1.2.1. 4-Hydroxy-6-nitro-2H-chromen-2-one (**5**). A mixture of **4** (6.17 mmol), potassium nitrate (7.71 mmol) in concentrated sulphuric acid (22 mL) was stirred at 0 $^\circ\text{C}$. After 24 h, the reaction was quenched with ice, affording the formation of a precipitate, which was filtered and dried. The resulting solid was purified by flash column chromatography, using as mobile phase a mixture of

CH₂Cl₂/EtOAc (8:2). 85% yield. ¹H-NMR (d₆-acetone, 250 MHz) δ: 8.54 (d, 1H, J= 2.25 Hz), 8.45 (dd, 1H, J= 2.5, 8.46 Hz), 7.62 (d, 1H, J= 7.62 Hz), 5.71 (s, 1H). ¹³C-NMR (d₆-acetone, 63 MHz) δ: 164.9, 161.1, 157.4, 143.3, 127.3, 119.5, 118.4, 116.7, 92.3.

6.1.2.2. 6-Amino-4-hydroxy-2H-chromen-2-one (6). A mixture of **5** (1.45 mmol), iron powder (10.03 mmol), and concentrated HCl (1.5 mL) in a mixture of ethanol, acetic acid and water (20 mL, 2:2:1) was stirred at room temperature for 1 h. The solution was diluted with water (50 mL), filtered through Celite and washed with water. The aqueous layers were neutralized with a saturated aqueous bicarbonate to pH 5-6, and extracted with ethyl acetate (3x100 mL). The combined organic layers were evaporated under reduced pressure to give a white solid in 93% yield. ¹H-NMR (d₆-acetone, 250 MHz) δ: 11.99 (s, 1H), 7.08 (d, 1H, J= 7.08 Hz), 6.96 (d, 1H, J= 2.5 Hz), 6.88 (dd, 1H, J= 7.08, 2.5 Hz), 5.51 (s, 1H), 3.38 (s, 2H).

6.1.3. General procedure for coupling reaction to obtain **15-23**

A mixture of the suitable 2-bromo-1,4-naphthoquinone **7-14** (0.79 mmol), copper(II) acetate (2.38 mmol), the proper coumarin **4** or **6** (2.38 mmol) and potassium carbonate (2.38 mmol) in acetonitrile (25 mL) was stirred at room temperature under nitrogen atmosphere overnight. After removing the solvent under reduced pressure, the corresponding crude products were purified as specified below.

6.1.3.1. 6H-naphtho[2',3':4,5]furo[3,2-c]chromene-6,7,12-trione (15). The title compound was obtained according to the general procedure using **7** and **4**. The crude mixture was diluted with water (20 mL) and extracted with dichloromethane (3x50 mL). The collected organic fractions were washed with brine, dried over Na₂SO₄ and evaporated under reduced pressure. The resulting residue was purified by flash column chromatography, using as mobile phase a mixture of CH₂Cl₂/Toluene/EtOAc (8:1.5:0.5). Compound **15** was obtained as a yellow solid in 36% yield.

¹H-NMR (400 MHz, d₆-DMSO): δ 7.82-7.86 (m, 1H), δ 7.92-7.94 (m, 1H), δ 8.01-8.03 (m, 1H), δ 8.08-8.22 (m, 1H), δ 8.23-8.27 (m, 2H), δ 8.45-8.49 (m, 2H). M.p. 230-232 °C (decomp); MS (ESI⁺) m/z: 317 [M+H]⁺, 339 [M+Na]⁺. ESI-MS C₁₉H₉O₅ found: 317.0456, calculated: 317.0450; C₁₉H₈NaO₅ found: 339.0260, calculated: 339.0269.

6.1.3.2. *6H-anthra[2',3':4,5]furo[3,2-c]chromene-6,7,14-trione* (**16**). The title compound was obtained according to the general procedure using **8** and **4**. The crude mixture was diluted with water (20 mL) and extracted with dichloromethane (3x50 mL). The collected organic fractions were washed with brine, dried over Na₂SO₄ and evaporated under reduced pressure. The resulting residue was purified by flash column chromatography, using as mobile phase a mixture of CH₂Cl₂/Toluene/MeOH (7.5:2:0.1). Compound **16** was obtained as a yellow solid in 28% yield. M.p. 249-251 °C (decomp); MS (ESI⁺) m/z: 389 [M+Na]⁺. ESI-MS C₂₃H₁₁O₅ found: 367.0603, calculated: 367.0606; C₂₃H₁₀NaO₅ found: 389.0421, calculated: 389.0426.

6.1.3.3. *11-Methoxy-6H-naphtho[2',3':4,5]furo[3,2-c]chromene-6,7,12-trione* (**17**). The title compound was obtained according to the general procedure using **9** and **4**. The crude mixture was diluted with water (20 mL) and extracted with dichloromethane (3x50 mL). The collected organic fractions were washed with brine, dried over Na₂SO₄ and evaporated under reduced pressure. The resulting residue was purified by filtration through pad of silica, using a mixture of CH₂Cl₂/Toluene/ EtOAc (7.5:1.5:1). Compound **17** was obtained as a yellow solid in 57% yield. ¹H-NMR (400 MHz, d₆-DMSO): δ 3.96 (s, 3H), δ 7.48-7.52 (m, 1H), δ 7.57-7.62 (m, 2H), δ 7.73-7.75 (m, 2H), δ 7.82-7.86 (m, 1H), δ 8.09 (dd, J = 1.6, 8.0 Hz, 1H). M.p. 216-218 °C (decomp); MS (ESI⁺) m/z: 347 [M+H]⁺. ESI-MS C₂₀H₁₁O₆ found: 347.0538, calculated: 347.0556.

6.1.3.4. *8-Methoxy-6H-naphtho[2',3':4,5]furo[3,2-c]chromene-6,7,12-trione* (**18**). The title compound was obtained according to the general procedure using **10** and **4**. The crude mixture was

diluted with water (20 mL) and extracted with dichloromethane (3x50 mL). The collected organic fractions were washed with brine, dried over Na₂SO₄ and evaporated under reduced pressure. The resulting residue was purified by filtration through a pad of silica, using a mixture of CH₂Cl₂/Toluene/ EtOAc (7.5:2:0.5). Compound **18** was obtained as a yellow solid in 16% yield.

¹H-NMR (400 MHz, d₆-DMSO): δ 3.95 (s, 3H), δ 7.49-7.53 (m, 1H), δ 7.58-7.64 (m, 2H), δ 7.74-7.78 (m, 2H), δ 7.82-7.86 (m, 1H), δ 8.12 (dd, *J* = 1.6, 9.6 Hz, 1H). M.p. 207-209 °C (decomp); MS (ESI⁺) *m/z*: 347 [M+H]⁺, 369 [M+Na]⁺. ESI-MS C₂₀H₁₁O₆ found: 347.0545, calculated: 347.0556; ESI-MS C₂₀H₁₀NaO₆ found: 369.0367, calculated: 369.0375.

6.1.3.5. *11-Hydroxy-6H-naphtho[2',3':4,5]furo[3,2-c]chromene-6,7,12-trione (19)*. The title compound was obtained according to the general procedure using **11** and **4**. The crude mixture was diluted with water (20 mL), acidified with 2N HCl until pH 5-6, and then extracted with dichloromethane (3x50 mL). The collected organic fractions were washed with brine, dried over Na₂SO₄ and evaporated under reduced pressure. The resulting residue was purified by flash column chromatography, using as mobile phase a mixture of CH₂Cl₂/EtOAc (9.9:0.1). Compound **19** was obtained as an orange solid in 30% yield. ¹H-NMR (400 MHz, CDCl₃): δ 7.34 (dd, *J* = 1.2, 8.8 Hz, 1H), δ 7.45-7.49 (m, 1H), δ 7.53 (d, *J* = 8.0 Hz, 1H), δ 7.69-7.74 (m, 2H), δ 7.86 (dd, *J* = 1.2, 7.6 Hz, 1H), δ 8.14 (dd, *J* = 1.2, 8.0 Hz, 1H), δ 11.85 (br s, exch, 1H). M.p. 214-216 °C (decomp); MS (ESI⁺) *m/z*: 355 [M+Na]⁺. ESI-MS C₁₉H₉O₆ found: 333.0388, calculated: 333.0399; C₁₉H₈NaO₆ found: 355.0214, calculated: 355.0219.

6.1.3.6. *8-Hydroxy-6H-naphtho[2',3':4,5]furo[3,2-c]chromene-6,7,12-trione (20)*. The title compound was obtained according to the general procedure using **12** and **4**. The crude mixture was diluted with water (20 mL), acidified with 2N HCl until pH 5-6, and then extracted with dichloromethane (3x50 mL). The collected organic fractions were washed with brine, dried over Na₂SO₄ and evaporated under reduced pressure. The resulting residue was purified by flash column

chromatography, using as mobile phase a mixture of CH₂Cl₂/EtOAc (9.95:0.05). Compound **20** was obtained as an orange solid in 30% yield. ¹H-NMR (400 MHz, CDCl₃): δ 7.38 (dd, *J* = 1.2, 8.4 Hz, 1H), δ 7.46-7.50 (m, 1H), δ 7.54 (d, *J* = 8.8 Hz, 1H), δ 7.68-7.74 (m, 2H), δ 7.84 (dd, *J* = 1.2, 7.2 Hz, 1H), δ 8.14 (dd, *J* = 1.2, 8.0 Hz, 1H), δ 12.28 (br, exch, 1H). M.p. 205-207 °C (decomp); MS (ESI⁺) *m/z*: 355 [M+Na]⁺. ESI-MS C₁₉H₉O₆ found: 333.0395, calculated: 333.0399; C₁₉H₈NaO₆ found: 355.0221, calculated: 355.0219.

6.1.3.7. *11-Acetoxy-6H-naphtho[2',3':4,5]furo[3,2-c]chromene-6,7,12-trione* (**21**). The title compound was obtained according to the general procedure using **13** and **4**. The crude mixture was diluted with water (20 mL) and extracted with dichloromethane (3x50 mL). The collected organic fractions were washed with brine, dried over Na₂SO₄ and evaporated under reduced pressure. The resulting residue was purified by flash column chromatography, using as mobile phase a mixture of CH₂Cl₂/EtOAc (9:1). Compound **21** was obtained as a yellow solid in 35% yield. ¹H-NMR (400 MHz, d₆-DMSO): δ 2.40 (s, 3H), δ 7.52 (t, *J* = 7.6 Hz, 1H), δ 7.59-7.65 (m, 2H), δ 7.75-7.80 (m, 1H), δ 7.96 (t, *J* = 7.6 Hz, 1H), δ 8.08-8.11 (m, 2H). M.p. 235-237 °C (decomp); MS (ESI⁺) *m/z*: 397 [M+Na]⁺. ESI-MS C₂₁H₁₁O₇ found: 375.0539, calculated: 375.0505; C₂₁H₁₀NaO₇ found: 397.0342, calculated: 397.0324.

6.1.3.8. *8-Acetoxy-6H-naphtho[2',3':4,5]furo[3,2-c]chromene-6,7,12-trione* (**22**). The title compound was obtained according to the general procedure using **14** and **4**. The crude mixture was diluted with water (20 mL) and extracted with dichloromethane (3x50 mL). The collected organic fractions were washed with brine, dried over Na₂SO₄ and evaporated under reduced pressure. The resulting residue was purified by flash column chromatography, using as mobile phase a mixture of CH₂Cl₂/EtOAc (9:1). Compound **22** was obtained as a yellow solid in 35% yield. ¹H-NMR (400 MHz, CDCl₃): δ 2.54 (s, 3H), δ 7.44-7.48 (m, 2H), δ 7.52 (d, *J* = 8.4 Hz, 1H), δ 7.70 (t, *J* = 8.0 Hz, 1H), δ 7.82 (t, *J* = 7.2 Hz, 1H), δ 8.13 (d, *J* = 7.6 Hz, 1H), δ 8.25 (d, *J* = 7.2 Hz, 1H). M.p. 221-223

°C (decomp); MS (ESI⁺) m/z: 397 [M+Na]⁺. ESI-MS C₂₁H₁₁O₇ found: 375.0499, calculated: 375.0505; C₂₁H₁₀NaO₇ found: 397.0335, calculated: 397.0324.

6.1.3.9. 2-Amino-11-hydroxy-6H-naphtho[2',3':4,5]furo[3,2-c]chromene-6,7,12-trione (23). The title compound was obtained according to the general procedure using **11** and **6**. The crude mixture was diluted with water (20 mL), acidified with 2N HCl until pH 5-6, and then extracted with ethyl acetate (1x80 mL). The collected organic fractions were washed with brine, dried over Na₂SO₄ and evaporated under reduced pressure. The resulting residue was purified by flash column chromatography, using as mobile phase a mixture of CH₂Cl₂/EtOAc (8.5:1.5). Compound **23** was obtained as a white-orange solid in 40% yield. ¹H-NMR (d₆-acetone, 250 MHz) δ: 7.94 (dd, 1H, J= 7.94 and 7.50 Hz), 7.62-7.55 (m, 1H), 7.36-7.32 (m, 2H), 7.23-7.18 (m, 1H), 6.97-6.93 (m, 1H), 6.00 (s, 1H). ¹³C-NMR (d₆-acetone, 63 MHz) δ: 211.4, 209.3, 167.9, 166.2, 154.1, 143.7, 133.1, 126.9, 124.7, 124.1, 117.7, 117.4, 117.1, 116.9, 116.8, 116.4, 107.9, 106.4, 92.1. ESI-MS C₁₉H₉NO₆ found: 347.0504, calculated: 347.0430.

6.2. Docking studies

6.2.1. Ligand preparation

Ligands were prepared with the LigPrep 3.6 tool available in the Schrödinger Suite 2015-4 and their ionization states were generated at pH 7.0 ± 2.0 with Epik 3.4.

6.2.2. Protein preparation

The X-ray coordinates of TcTR and TbGAPDH were retrieved from the Protein Data Bank (PDB codes 1BZL and 2X0N, respectively). To build more representative binding pockets of TcTR and TbGAPDH, their structures were compared and modeled to the structures of TbTR in complex with 3,4-dihydroquinazoline inhibitor (PDB 2WPF) and TcGAPDH in complex with chalepin downloadable in the Protein Data Bank (PDB 1K3T).

All the structures were then processed with the Protein Preparation Wizard tool. Water molecules, cofactors, ligands and ions were removed, and an exhaustive sampling of the orientations of groups, whose hydrogen-bonding network needed to be optimized, was performed. Finally, the protein structure was refined by minimization with the OPLS2005 force field until a final RMSD of 0.30 Å compared to the input protein coordinates.

6.2.3. Docking

Docking studies were carried out with the Glide software 6.9 within the Schrödinger Suite 2015-4. The prepared protein structures were then used to build the energy grid with Grid Generation tool of the Schrödinger Suite 2015-4. In particular, chain C was selected for *Tb*GAPDH and chains A and B were chosen for *Tc*TR to calculate the grid, whose enclosing box was centered on the co-crystallized ligands. For *Tb*GAPDH, a size of 10 Å and 30 Å was used for the INNERBOX and OUTERBOX, respectively, whereas for *Tc*TR grid dimensions of 12 Å and 30 Å were employed. The VdW radii of ligand atoms were scaled by 0.8 and the charge cut-off for polarity was set at 0.1. All other parameters were used as default values. Extra Precision (XP) Glide was used to dock and score compounds. Ten different poses per ligand were saved, sorted by GlideScore, and visually inspected. The best-ranked protein-ligand complexes were then minimized using Prime MM-GBSA with the OPLS2005 force field, considering flexible residues at a distance of 6 Å from ligand. Pictures were generated with Maestro 10.4.

6.3. Biological evaluation

6.3.1. *Tb*GAPDH inhibition assays

Recombinant *Tb*GAPDH was expressed and purified in the laboratory of Professor Fato (FaBiT Department, University of Bologna), as previously described [18, 28], with minor modifications.

*Tb*GAPDH activity was assayed spectrophotometrically by following NAD^+ reduction at 340 nm in triethanolamine (TEA) buffer (10 mM TEA, 1.7 mM NaHCO_3 , 100 mM KCl, 5 mM MgSO_4 , and 1 mM ethylenediaminetetraacetic acid (EDTA)) pH 7.6 at 25 °C, as reported by Wiggers et al [48].

The reaction mixtures included TEA buffer, pH 7.6, *Tb*GAPDH (ranging from 200 to 300 µg of protein), 400 µM NAD^+ , 500 µM KH_2PO_4 , 300 µM GAP, and varying concentrations of inhibitors in a total volume of 1 mL. Stock solutions of the inhibitors were prepared in 100% DMSO (v/v). Inhibition data are presented as percentage of GAPDH activity. Experiments were carried out in triplicate.

6.3.2. *Tc*TR inhibition assays and kinetic analysis

Trypanothione disulfide (TS_2) and recombinant *Tc*TR were prepared according to published procedures [32, 49]. Stock solutions of the inhibitors were prepared in DMSO (v/v). The kinetic analyses were performed by using a Jasco V650 spectrophotometer. The activity of *Tc*TR was measured at 25 °C in a total volume of 1 mL assay buffer (40 mM HEPES, 1 mM EDTA, pH 7.5 [33]) containing 100 µM NADPH and 5-10 mU enzyme in the absence and presence of the inhibitor. Each assay contained a total of 5% DMSO (v/v). The reaction was started by adding TS_2 , and NADPH consumption was followed at 340 nm. The type of inhibition was derived from the respective Lineweaver-Burk plots. The activity of *Tc*TR was measured in the absence and presence of two fixed concentrations of inhibitor varying the concentration of TS_2 (20, 40, 60, 100 and 200 µM). The inhibitor constants were calculated from the direct plot using non-linear least-squares data fitting in Microsoft Excel [50, 51].

6.3.3. In-vitro evaluation of activity against *L. infantum* intramacrophage amastigotes

The compounds were tested at a single concentration of 5 (**16-18**, **20-22**), 10 (**19**), 12.5 (**15**) or 50 µM (**23**), according to their respective solubility. THP-1 cells were plated onto 384 well plates in RPMI complete media containing 50 ng/mL phorbol 12-myristate 13-acetate (PMA, Sigma-

Aldrich) and incubated for 48 h. Then, 6 day-old *Leishmania infantum* (strain MHOM/BR/72/BH046) promastigotes were added at a ratio 50 parasites per each THP-1 cell seeded earlier. After 24 h infection, negative controls (0.5% DMSO v/v), positive controls (10 μ M amphotericin B, Sigma-Aldrich) or compounds were added to the plate. Assay plates were incubated for 48 h, and then fixed 4% v/v paraformaldehyde and stained with Draq 5. The Operetta High-Content automated imaging system (PerkinElmer) was used to acquire images and the HarmonyTM software (PerkinElmer) was optimized to quantify: host cells number, infection ratio and number of parasites per infected cell. The ratio between infected cells and total number of cells was calculated, and defined as the Infection Ratio (IR). The raw data for IR values was normalized to negative – DMSO (mock)-treated infected cells – and positive (non – infected cells) controls to determine the normalized anti-parasitic activity.

6.3.4. In-vitro evaluation of activity against *T. brucei*

The efficacy of compounds against *T. b. brucei* strain Lister 427 bloodstream forms was evaluated at a single concentration ranging from 5 to 50 μ M, according to solubility and as mentioned above, using a SYBRTM Green based assay as previously described in literature [52]. Compounds were transferred from stock plates to assay plates throughout using an automated workstation (Janus MDT, PerkinElmer) yielding a final 0.5% of DMSO (v/v) i.e. a 200-fold dilution.

6.3.5. In-vitro evaluation of activity against *T. cruzi*

The efficacy of compounds against *T. cruzi* was evaluated at a single concentration ranging from 5 to 50 μ M, according to solubility and, as described above, following the procedure reported in the literature [53], with minor modifications. Infections were performed immediately after compound addition with 3,000 U2OS cells/well co-seeded with *T. cruzi* Y strain trypomastigotes at a 5:1 ratio and dispensed with the aid of a liquid handler (WellMate[®], Thermo Scientific Matrix[®]). Plates were subsequently incubated at 37 °C and 5% CO₂ for 72 h. Fixation and staining steps, Operetta image

acquisition, data processing and normalization were performed as described for the *L. infantum* assay above. The host toxicity value was calculated based on the following equation: host toxicity = $1 - (\text{CRS}/\text{CRN}) \times 100$; where CRS = cell ratio in compound/sample treated well and CRN = average cell ratio in negative control wells.

6.3.6. *In-vitro compound mediated early-toxicity assessment*

6.3.6.1. *Cytotoxicity assay against A549 cells*

The assay was accomplished using the Cell Titer-GloTM assay from Promega as described in the literature [54, 55]. Briefly, the assay detects cellular ATP content with the amount of ATP being directly proportional to the number of the present cells (A549 cells were obtained from DSMZ (German Collection of Microorganisms and Cell Cultures), Braunschweig, Germany. Paclitaxel was used as a positive control at 10 μM).

6.3.6.2. *hERG assay*

The hERG inhibition assay was performed using the Invitrogen PredictorTM hERG Fluorescence Polarisation Assay. Briefly, the assay uses a membrane fraction containing hERG channel (PredictorTM hERG Membrane) and a high-affinity red fluorescent hERG channel ligand, or “tracer” (PredictorTM hERG Tracer Red), whose displacement by test compounds can be determined in a homogenous, Fluorescence Polarization format, as described in the literature [54, 55].

6.3.6.3. *Cytochrome P450 1A2, 2C9, 2C19, 2D6 and 3A4 assays*

The CYP inhibition assays were carried out by means of the Promega P450-GloTM assay platform, as described in the literature [54, 55]. Briefly, action of the CYP450 enzymes upon each substrate results in the generation of light and a light decrease was indicative of inhibition of the enzymes.

6.3.6.4. *Mitochondrial toxicity assay*

This assay employed the MitoTracker[®] Red chloromethyl-Xrosamine (CMXRos) that stains mitochondria in live cells. Briefly, 786-O cells (CLS Cell Lines Service GmbH, Germany) were maintained using RPMI-1640 medium containing 2 mM glutamine, FCS (10% v/v), streptomycin (100 mg/mL) and penicillin G (100 U/mL) and imaged after addition of CMXRos using an High Content Imaging (Opera[™], PerkinElmer) as described in the literature [54, 55]. Valinomycin was used at 100 nM concentration.

Acknowledgments

This work was supported by MIUR, Rome (PRIN Funds 201274BNKN_003) and the University of Bologna (RFO 2015). The anti-parasitic activity and the early-toxicity profiling of the compounds were developed within the international collaborative effort of the European Union's Seventh Framework Programme for research, technological development and demonstration under grant agreement n° 603240 (NMTrypI—New Medicines for Trypanosomatidic Infections) <http://www.nmtrypi.eu/>. G.F. thanks the COST Action CM-1307 “Targeted chemotherapy towards diseases caused by endoparasites” of the EC for a STSM grant that enabled her to work for two months in the laboratory of R.L.K.S. at the Biochemistry Center (BZH) in Heidelberg. The authors would like also to acknowledge the contribution of the COST Action CA15135 “Multi-target paradigm for innovative ligand identification in the drug discovery process (MuTaLig)”. We are also thankful to Centro Interdipartimentale Grandi Strumenti (CIGS) of the University of Modena. Funding from Spain (MICINN, SAF2015-6690-R) is gratefully acknowledged (M.T.M.).

References

- [1] M.C. Field, D. Horn, A.H. Fairlamb, M.A. Ferguson, D.W. Gray, K.D. Read, M. De Rycker, L.S. Torrie, P.G. Wyatt, S. Wyllie, I.H. Gilbert, Anti-trypanosomatid drug discovery: an ongoing challenge and a continuing need, *Nat. Rev. Microbiol.*, 15 (2017) 217-231.

- [2] L.S. Goupil, J.H. McKerrow, Introduction: drug discovery and development for neglected diseases, *Chem. Rev.*, 114 (2014) 11131-11137.
- [3] A.S. Nagle, S. Khare, A.B. Kumar, F. Supek, A. Buchynskyy, C.J. Mathison, N.K. Chennamaneni, N. Pendem, F.S. Buckner, M.H. Gelb, V. Molteni, Recent developments in drug discovery for leishmaniasis and human African trypanosomiasis, *Chem. Rev.*, 114 (2014) 11305-11347.
- [4] P.D. Ready, Epidemiology of visceral leishmaniasis, *Clin. Epidemiol.*, 6 (2014) 147-154.
- [5] P.M. Cheuka, G. Mayoka, P. Mutai, K. Chibale, The Role of Natural Products in Drug Discovery and Development against Neglected Tropical Diseases, *Molecules*, 22 (2016).
- [6] D.J. Newman, G.M. Cragg, Natural Products as Sources of New Drugs from 1981 to 2014, *J. Nat. Prod.*, 79 (2016) 629-661.
- [7] A.L. Harvey, R.L. Clark, S.P. Mackay, B.F. Johnston, Current strategies for drug discovery through natural products, *Expert Opin. Drug Dis.*, 5 (2010) 559-568.
- [8] A.L. Harvey, R. Edrada-Ebel, R.J. Quinn, The re-emergence of natural products for drug discovery in the genomics era, *Nat. Rev. Drug Discov.*, 14 (2015) 111-129.
- [9] A. Cavalli, M.L. Bolognesi, Neglected tropical diseases: multi-target-directed ligands in the search for novel lead candidates against *Trypanosoma* and *Leishmania*, *J. Med. Chem.*, 52 (2009) 7339-7359.
- [10] A. Cavalli, F. Lizzi, S. Bongarzone, F. Belluti, L. Piazzzi, M.L. Bolognesi, Complementary medicinal chemistry-driven strategies toward new antitrypanosomal and antileishmanial lead drug candidates, *FEMS Immunol. Med. Microbiol.*, 58 (2010) 51-60.
- [11] H.F. Ji, X.J. Li, H.Y. Zhang, Natural products and drug discovery. Can thousands of years of ancient medical knowledge lead us to new and powerful drug combinations in the fight against cancer and dementia?, *EMBO Rep.*, 10 (2009) 194-200.
- [12] F. Belluti, E. Uliassi, G. Veronesi, C. Bergamini, M. Kaiser, R. Brun, A. Viola, R. Fato, P.A. Michels, R.L. Krauth-Siegel, A. Cavalli, M.L. Bolognesi, Toward the development of dual-targeted

glyceraldehyde-3-phosphate dehydrogenase/trypanothione reductase inhibitors against *Trypanosoma brucei* and *Trypanosoma cruzi*, ChemMedChem, 9 (2014) 371-382.

[13] M. Gualdrón-López, P.A.M. Michels, W. Quiñones, A.J. Cáceres, L. Avilán, J.-L. Concepción, Function of Glycosomes in the Metabolism of Trypanosomatid Parasites and the Promise of Glycosomal Proteins as Drug Targets, in: Trypanosomatid Diseases, Wiley-VCH Verlag GmbH & Co. KGaA, 2013, pp. 121-151.

[14] A. Ilari, A. Fiorillo, I. Genovese, G. Colotti, Polyamine-trypanothione pathway: an update, Future Med. Chem., 9 (2017) 61-77.

[15] J.G. Tangmouo, A.L. Meli, J. Komguem, V. Kuete, F.N. Ngounou, D. Lontsi, V.P. Beng, M.I. Choudhary, B.L. Sondengam, Crassiflorone, a new naphthoquinone from *Diospyros crassiflora* (Hien), Tetrahedron Lett., 47 (2006) 3067-3070.

[16] V. Kuete, J.G. Tangmouo, J.J.M. Meyer, N. Lall, Diospyrone, crassiflorone and plumbagin: three antimycobacterial and antigonorrhoeal naphthoquinones from two *Diospyros* spp., Int. J. Antimicrob. Ag., 34 (2009) 322-325.

[17] F. Lizzi, G. Veronesi, F. Belluti, C. Bergamini, A. Lopez-Sanchez, M. Kaiser, R. Brun, R.L. Krauth-Siegel, D.G. Hall, L. Rivas, M.L. Bolognesi, Conjugation of quinones with natural polyamines: toward an expanded antitrypanosomatid profile, J. Med. Chem., 55 (2012) 10490-10500.

[18] S. Pieretti, J.R. Haanstra, M. Mazet, R. Perozzo, C. Bergamini, F. Prati, R. Fato, G. Lenaz, G. Capranico, R. Brun, B.M. Bakker, P.A. Michels, L. Scapozza, M.L. Bolognesi, A. Cavalli, Naphthoquinone derivatives exert their antitrypanosomal activity via a multi-target mechanism, PLoS Negl. Trop. Dis., 7 (2013) e2012.

[19] M.C. Taylor, J.M. Kelly, C.J. Chapman, A.H. Fairlamb, M.A. Miles, The Structure, Organization, and Expression of the *Leishmania Donovanii* Gene Encoding Trypanothione Reductase, Mol. Biochem. Parasit., 64 (1994) 293-301.

- [20] V. Hannaert, F.R. Opperdoes, P.A. Michels, Glycosomal glyceraldehyde-3-phosphate dehydrogenase of *Trypanosoma brucei* and *Trypanosoma cruzi*: expression in *Escherichia coli*, purification, and characterization of the enzymes, *Protein Expr. Purif.*, 6 (1995) 244-250.
- [21] F.M. Vellieux, J. Hajdu, C.L. Verlinde, H. Groendijk, R.J. Read, T.J. Greenhough, J.W. Campbell, K.H. Kalk, J.A. Littlechild, H.C. Watson, et al., Structure of glycosomal glyceraldehyde-3-phosphate dehydrogenase from *Trypanosoma brucei* determined from Laue data, *Proc. Natl. Acad. Sci. U.S.A.*, 90 (1993) 2355-2359.
- [22] C.S. Bond, Y. Zhang, M. Berriman, M.L. Cunningham, A.H. Fairlamb, W.N. Hunter, Crystal structure of *Trypanosoma cruzi* trypanothione reductase in complex with trypanothione, and the structure-based discovery of new natural product inhibitors, *Structure*, 7 (1999) 81-89.
- [23] J. Padwal, W. Lewis, C.J. Moody, Synthesis of the Reported Structure of Crassiflorone, a Pentacyclic Naphthoquinone Isolated from the African Ebony *Diospyros crassiflora*, *Synlett.*, (2010) 514-516.
- [24] J. Padwal, W. Lewis, C.J. Moody, Synthesis of the reported structure of crassiflorone, a naturally occurring quinone isolated from the African ebony *Diospyros crassiflora*, and regioisomeric pentacyclic furocoumarin naphthoquinones, *Org. Biomol. Chem.*, 9 (2011) 3484-3493.
- [25] C.N. Huang, P.Y. Kuo, C.H. Lin, D.Y. Yang, Synthesis and characterization of 2H-pyrano[3,2-c]coumarin derivatives and their photochromic and redox properties, *Tetrahedron*, 63 (2007) 10025-10033.
- [26] M.L. Bolognesi, F. Lizzi, R. Perozzo, R. Brun, A. Cavalli, Synthesis of a small library of 2-phenoxy-1,4-naphthoquinone and 2-phenoxy-1,4-anthraquinone derivatives bearing anti-trypanosomal and anti-leishmanial activity, *Bioorg. Med. Chem. Lett.*, 18 (2008) 2272-2276.
- [27] R.C. Montenegro, A.J. Araujo, M.T. Molina, J.D. Marinho Filho, D.D. Rocha, E. Lopez-Montero, M.O. Goulart, E.S. Bento, A.P. Alves, C. Pessoa, M.O. de Moraes, L.V. Costa-Lotufo,

Cytotoxic activity of naphthoquinones with special emphasis on juglone and its 5-O-methyl derivative, *Chem. Biol. Interact.*, 184 (2010) 439-448.

[28] F. Prati, C. Bergamini, M.T. Molina, F. Falchi, A. Cavalli, M. Kaiser, R. Brun, R. Fato, M.L. Bolognesi, 2-Phenoxy-1,4-naphthoquinones: From a Multitarget Antitrypanosomal to a Potential Antitumor Profile, *J. Med. Chem.*, 58 (2015) 6422-6434.

[29] F.V. Maluf, A.D. Andricopulo, G. Oliva, R.V. Guido, A pharmacophore-based virtual screening approach for the discovery of *Trypanosoma cruzi* GAPDH inhibitors, *Future Med. Chem.*, 5 (2013) 2019-2035.

[30] F.C. Herrmann, M. Lenz, J. Jose, M. Kaiser, R. Brun, T.J. Schmidt, In Silico Identification and in Vitro Activity of Novel Natural Inhibitors of *Trypanosoma brucei* Glyceraldehyde-3-phosphate-dehydrogenase, *Molecules*, 20 (2015) 16154-16169.

[31] V.E. Cornelio, F.V. Maluf, J.B. Fernandes, M.F.G. da Silva, G. Oliva, R.V. Guidob, P.C. Vieira, Isolation of Tiliroside from *Spiranthera odoratissima* as Inhibitor of *Trypanosoma cruzi* Glyceraldehyde-3-phosphate Dehydrogenase by Using Bioactivity-Guided Fractionation, *J. Braz. Chem. Soc.*, 28 (2017) 512-519.

[32] F.X. Sullivan, C.T. Walsh, Cloning, sequencing, overproduction and purification of trypanothione reductase from *Trypanosoma cruzi*, *Mol. Biochem. Parasitol.*, 44 (1991) 145-147.

[33] M.C. Jockers-Scherubl, R.H. Schirmer, R.L. Krauth-Siegel, Trypanothione reductase from *Trypanosoma cruzi*. Catalytic properties of the enzyme and inhibition studies with trypanocidal compounds, *Eur. J. Biochem.*, 180 (1989) 267-272.

[34] T.J. Benson, J.H. McKie, J. Garforth, A. Borges, A.H. Fairlamb, K.T. Douglas, Rationally designed selective inhibitors of trypanothione reductase. Phenothiazines and related tricyclics as lead structures, *Biochem. J.*, 286 (Pt 1) (1992) 9-11.

[35] E. Persch, S. Bryson, N.K. Todoroff, C. Eberle, J. Thelemann, N. Dirdjaja, M. Kaiser, M. Weber, H. Derbani, R. Brun, G. Schneider, E.F. Pai, R.L. Krauth-Siegel, F. Diederich, Binding to

large enzyme pockets: small-molecule inhibitors of trypanothione reductase, *ChemMedChem*, 9 (2014) 1880-1891.

[36] J.L. Bolton, M.A. Trush, T.M. Penning, G. Dryhurst, T.J. Monks, Role of quinones in toxicology, *Chem. Res. Toxicol.*, 13 (2000) 135-160.

[37] A.R. Renslo, J.H. McKerrow, Drug discovery and development for neglected parasitic diseases, *Nat. Chem. Biol.*, 2 (2006) 701-710.

[38] F.S. Buckner, Experimental chemotherapy and approaches to drug discovery for *Trypanosoma cruzi* infection, *Adv. Parasitol.*, 75 (2011) 89-119.

[39] P. Baranczewski, A. Stanczak, K. Sundberg, R. Svensson, A. Wallin, J. Jansson, P. Garberg, H. Postlind, Introduction to in vitro estimation of metabolic stability and drug interactions of new chemical entities in drug discovery and development, *Pharmacol. Rep.*, 58 (2006) 453-472.

[40] K. Seden, S. Khoo, D. Back, N. Prevatt, M. Lamorde, P. Byakika-Kibwika, J. Mayito, M. Ryan, C. Merry, Drug-drug interactions between antiretrovirals and drugs used in the management of neglected tropical diseases: important considerations in the WHO 2020 Roadmap and London Declaration on Neglected Tropical Diseases, *AIDS*, 27 (2013) 675-686.

[41] L. Jia, X. Liu, The conduct of drug metabolism studies considered good practice (II): in vitro experiments, *Curr. Drug Metab.*, 8 (2007) 822-829.

[42] E. Raschi, L. Ceccarini, F. De Ponti, M. Recanatini, hERG-related drug toxicity and models for predicting hERG liability and QT prolongation, *Expert Opin. Drug Metab. Toxicol.*, 5 (2009) 1005-1021.

[43] K. Salomao, N.A. De Santana, M.T. Molina, S.L. De Castro, R.F.S. Menna-Barreto, *Trypanosoma cruzi* mitochondrial swelling and membrane potential collapse as primary evidence of the mode of action of naphthoquinone analogues, *BMC Microbiol.*, 13 (2013).

[44] K. Wallace, A. Starkov, Mitochondrial targets of drug toxicity, *Annu. Rev. Pharmacol. Toxicol.*, 40 (2000) 353-388.

- [45] J.B. Baell, Feeling Nature's PAINS: Natural Products, Natural Product Drugs, and Pan Assay Interference Compounds (PAINS), *J. Nat. Prod.*, 79 (2016) 616-628.
- [46] D. Lagorce, O. Sperandio, J.B. Baell, M.A. Miteva, B.O. Villoutreix, FAF-Drugs3: a web server for compound property calculation and chemical library design, *Nucleic Acids Res.*, 43 (2015) W200-207.
- [47] A.D. Kwong, R.S. Kauffman, P. Hurter, P. Mueller, Discovery and development of telaprevir: an NS3-4A protease inhibitor for treating genotype 1 chronic hepatitis C virus, *Nat. Biotechnol.*, 29 (2011) 993-1003.
- [48] H.J. Wiggers, J. Cheleski, A. Zottis, G. Oliva, A.D. Andricopulo, C.A. Montanari, Effects of organic solvents on the enzyme activity of *Trypanosoma cruzi* glyceraldehyde-3-phosphate dehydrogenase in calorimetric assays, *Anal. Biochem.*, 370 (2007) 107-114.
- [49] M.A. Comini, N. Dirdjaja, M. Kaschel, R.L. Krauth-Siegel, Preparative enzymatic synthesis of trypanothione and trypanothione analogues, *Int. J. Parasitol.*, 39 (2009) 1059-1062.
- [50] A.M. Brown, A step-by step guide to non-linear regression analysis of experimental data using a Microsoft Excel spreadsheet, *FASEB J.*, 15 (2001) A747-A747.
- [51] G. Kemmer, S. Keller, Nonlinear least-squares data fitting in Excel spreadsheets, *Nat. Protoc.*, 5 (2010) 267-281.
- [52] J. Faria, C.B. Moraes, R. Song, B.S. Pascoalino, N. Lee, J.L. Siqueira-Neto, D.J. Cruz, T. Parkinson, J.R. Ioset, A. Cordeiro-da-Silva, L.H. Freitas-Junior, Drug discovery for human African trypanosomiasis: identification of novel scaffolds by the newly developed HTS SYBR Green assay for *Trypanosoma brucei*, *J. Biomol. Screen.*, 20 (2015) 70-81.
- [53] C.B. Moraes, M.A. Giardini, H. Kim, C.H. Franco, A.M. Araujo, S. Schenkman, E. Chatelain, L.H. Freitas, Nitroheterocyclic compounds are more efficacious than CYP51 inhibitors against *Trypanosoma cruzi*: implications for Chagas disease drug discovery and development, *Sci. Rep.*, 4 (2014).

- [54] C. Borsari, R. Luciani, C. Pozzi, I. Poehner, S. Henrich, M. Trande, A. Cordeiro-da-Silva, N. Santarem, C. Baptista, A. Tait, F. Di Pisa, L. Dello Iacono, G. Landi, S. Gul, M. Wolf, M. Kuzikov, B. Ellinger, J. Reinshagen, G. Witt, P. Gribbon, M. Kohler, O. Keminer, B. Behrens, L. Costantino, P.T. Nevado, E. Bifeld, J. Eick, J. Clos, J. Torrado, M.D. Jimenez-Anton, M.J. Corral, J.M. Alunda, F. Pellati, R.C. Wade, S. Ferrari, S. Mangani, M.P. Costi, Profiling of Flavonol Derivatives for the Development of Antitrypanosomatidic Drugs, *J. Med. Chem.*, 59 (2016) 7598-7616.
- [55] C. Borsari, N. Santarem, J. Torrado, A.I. Olias, M.J. Corral, C. Baptista, S. Gul, M. Wolf, M. Kuzikov, B. Ellinger, G. Witt, P. Gribbon, J. Reinshagen, P. Linciano, A. Tait, L. Costantino, L.H. Freitas-Junior, C.B. Moraes, P.B. dos Santos, L.M. Alcantara, C.H. Franco, C.D. Bertolacini, V. Fontana, P.T. Nevado, J. Clos, J.M. Alunda, A. Cordeiro-Da-Silva, S. Ferrari, M.P. Costi, Methoxylated 2'-hydroxychalcones as antiparasitic hit compounds, *Eur. J. Med. Chem.*, 126 (2017) 1129-1135.

Highlights

- New trypanocidal derivatives were designed from the natural compound crassiflorone
- These new compounds inhibited two trypanosomal targets: GAPDH and TR
- They displayed phenotypic cellular activity against *T. brucei* parasites
- They showed no toxicity towards human cells and mitochondria